



*Supplement of*

## **Co-emission of volcanic sulfur and halogens amplifies volcanic effective radiative forcing**

**John Staunton-Sykes et al.**

*Correspondence to:* John Staunton-Sykes (jjas3@cam.ac.uk) and Thomas J. Aubry (ta460@cam.ac.uk)

The copyright of individual parts of the supplement might differ from the article licence.

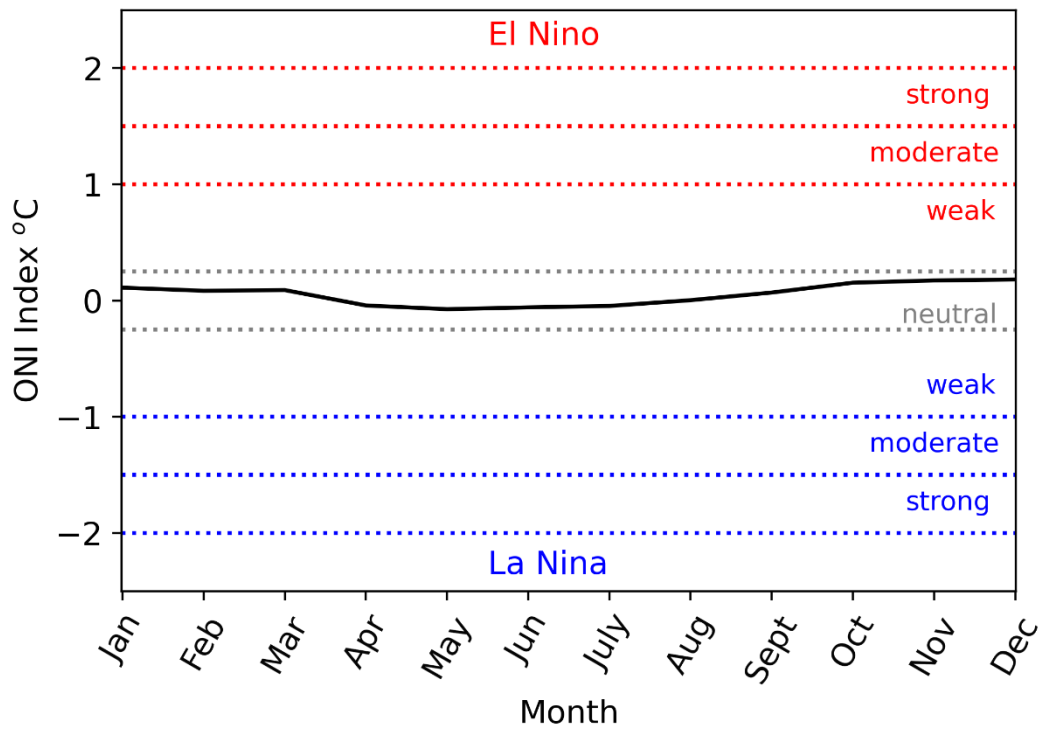
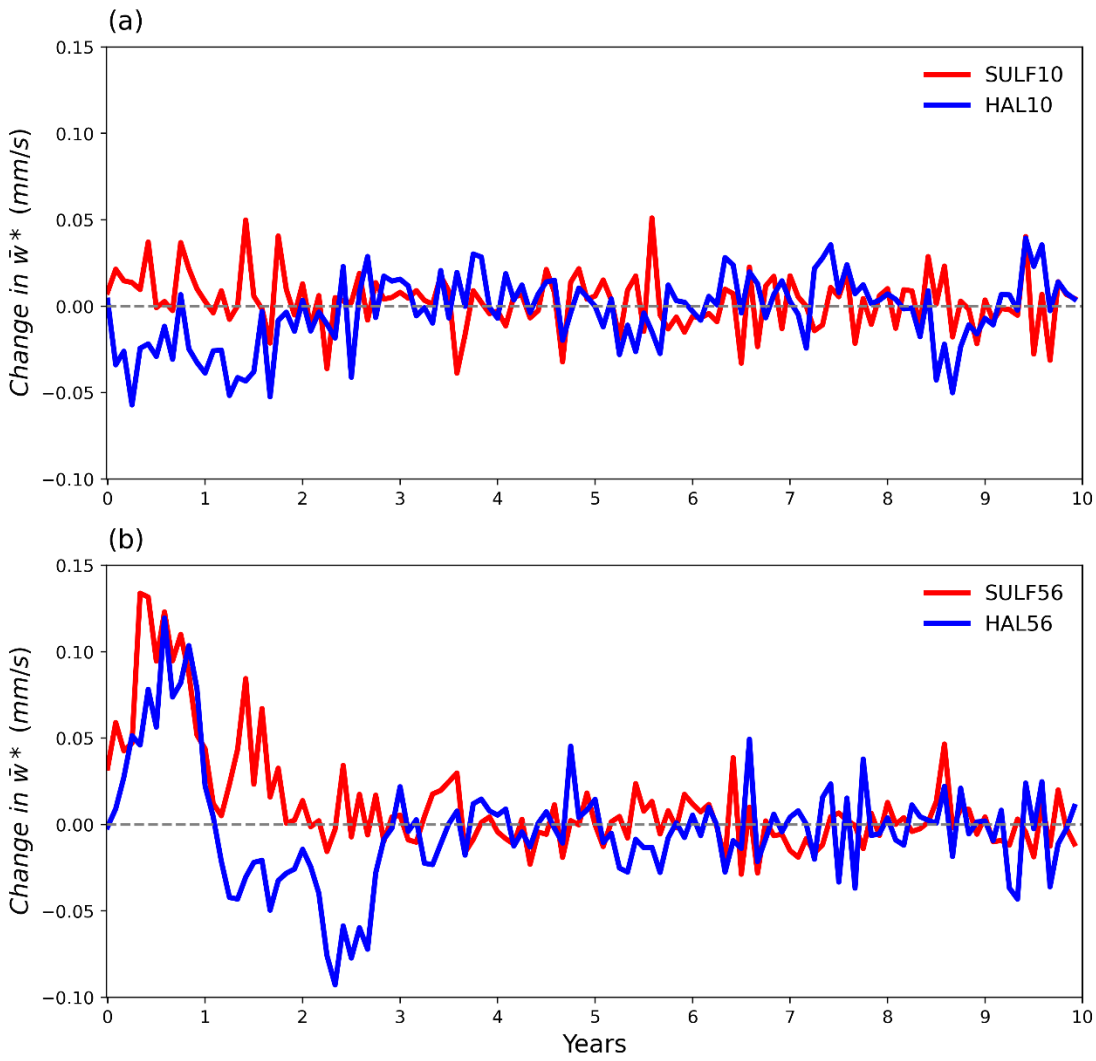
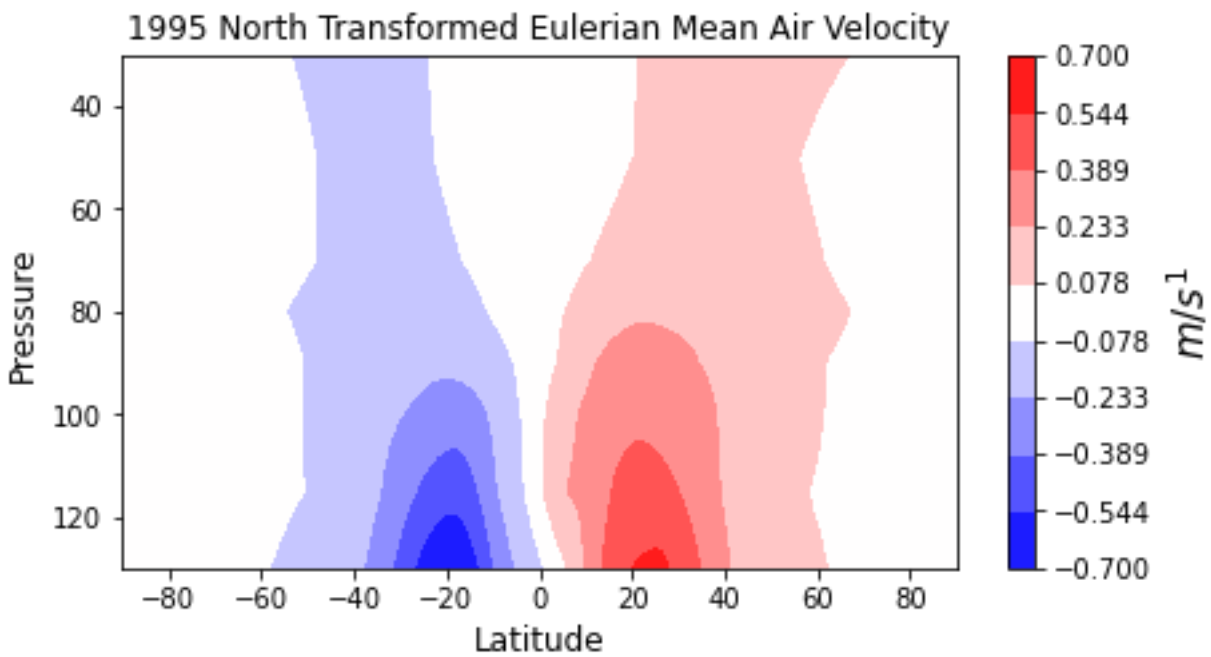


**Figure S1** The Oceanic Niño Index (ONI) of the prescribed SST used to force the atmosphere-only simulations. ONI is defined as the 3 month running mean of SST anomalies in the Niño 3.4 region (5N-5S, 120-170W) compared to the 1971- 2000 base period.

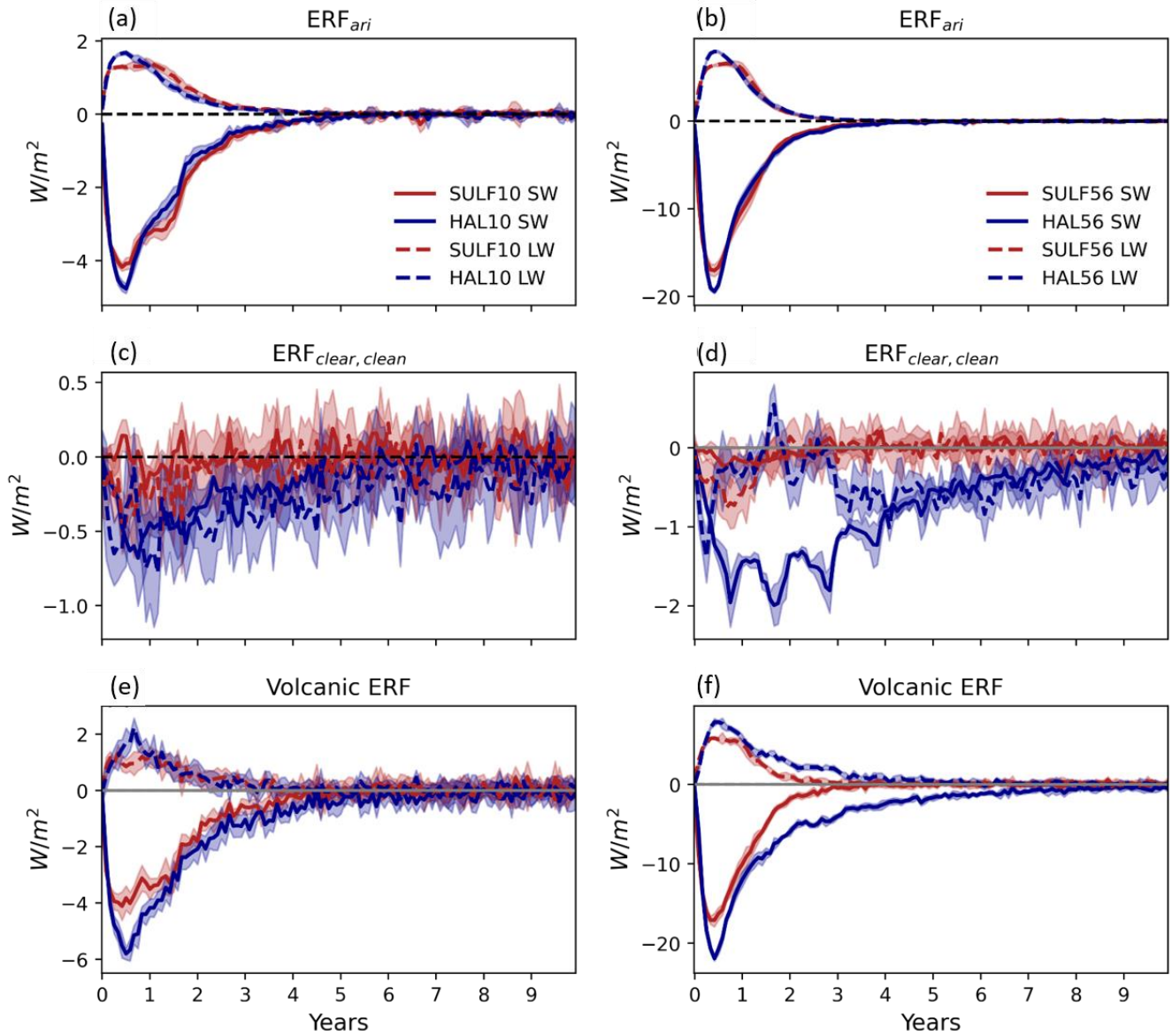


5

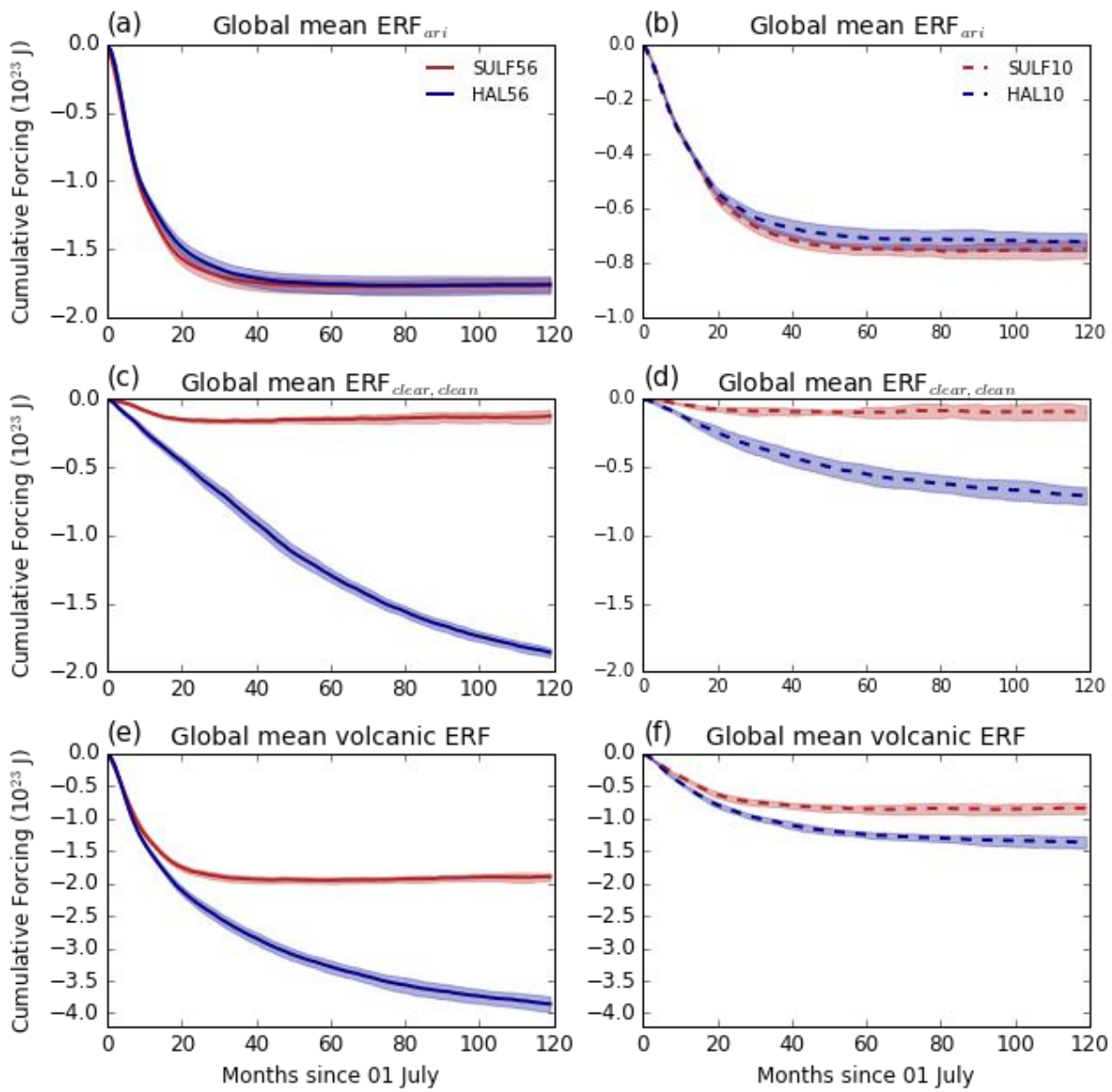
**Figure S2** Time series of change in 20°S – 20°N mean  $\bar{w}^*$  (residual mean vertical velocity) at 50 hPa for (a) SULF10 and HAL10, (b) SULF56 and HAL56 compared to the control climatology.



10 **Figure S3** Northward transformed eulerian mean air velocity ( $\text{ms}^{-1}$ ) in the control simulation, averaged over the full 20 years. The poleward velocity reduces with altitude.



15 **Figure S4** Global mean evolution of TOA  $\text{ERF}_{\text{ari}}$  (top),  $\text{ERF}_{\text{clear, clean}}$  (middle) and volcanic ERF (bottom), in SULF10 and HAL10 (left) and SULF56 and HAL56 (right). Sulfur-only (red), co-emission (blue), SW forcing (solid), LW forcing (dashed). Shading represents the ensemble range.



20 **Figure S5** Cumulative global mean TOA  $ERF_{ari}$  in SULF56 & HAL56 (a) and SULF10 & HAL10 (b),  $ERF_{clear, clean}$  in SULF56 & HAL56 (c) and SULF10 & HAL10 (d), Volcanic ERF in SULF56 & HAL56 (e) and SULF10 & HAL10 (f), Shading represents the ensemble range.

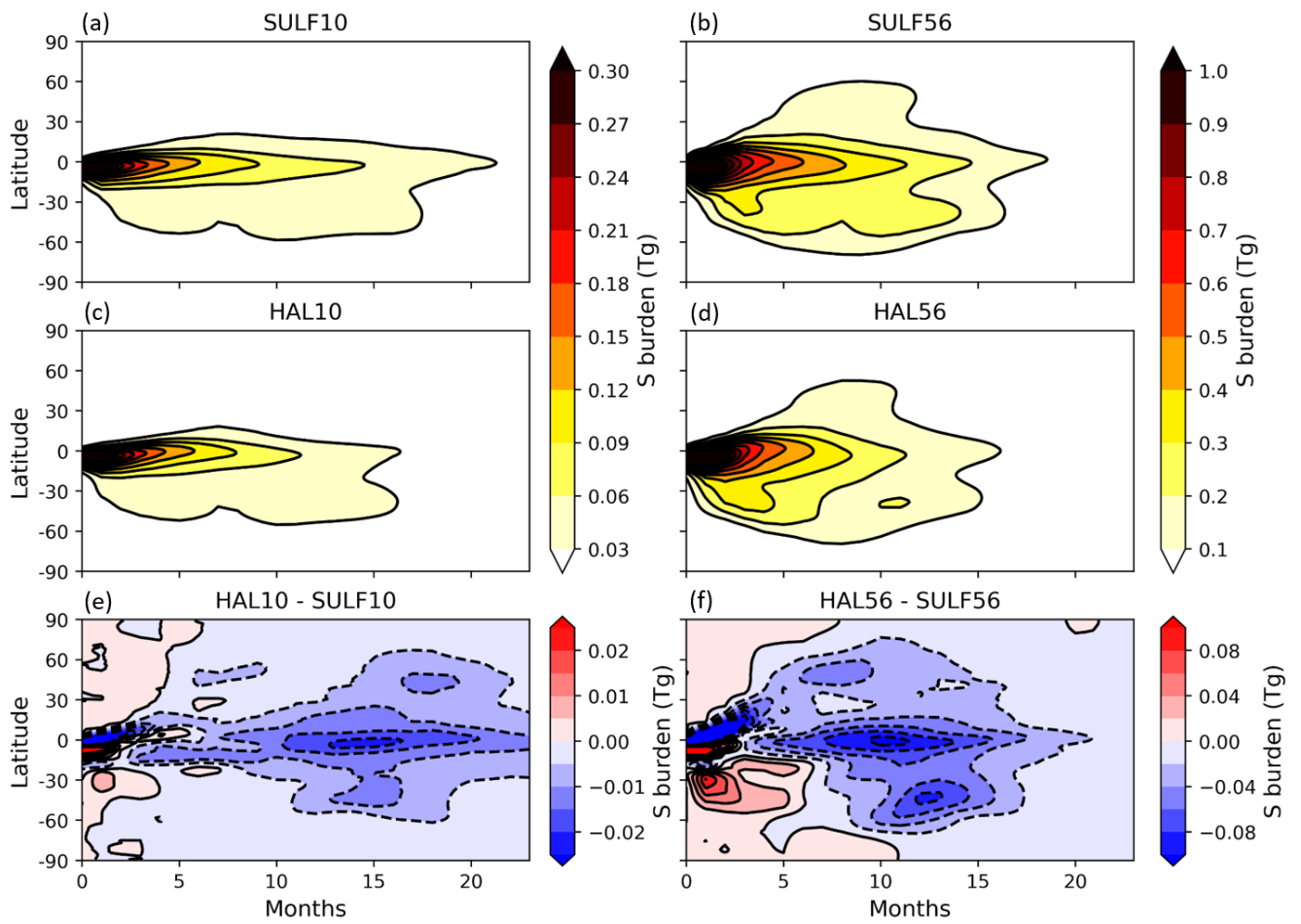


**Figure S6** Evolution of total sulfur burden, in SULF10 (a), SULF56 (b), HAL10 (c) and HAL56 (d). The HAL10 – SULF10 difference is shown in (e) and the HAL56 - SULF56 difference is shown in (f).

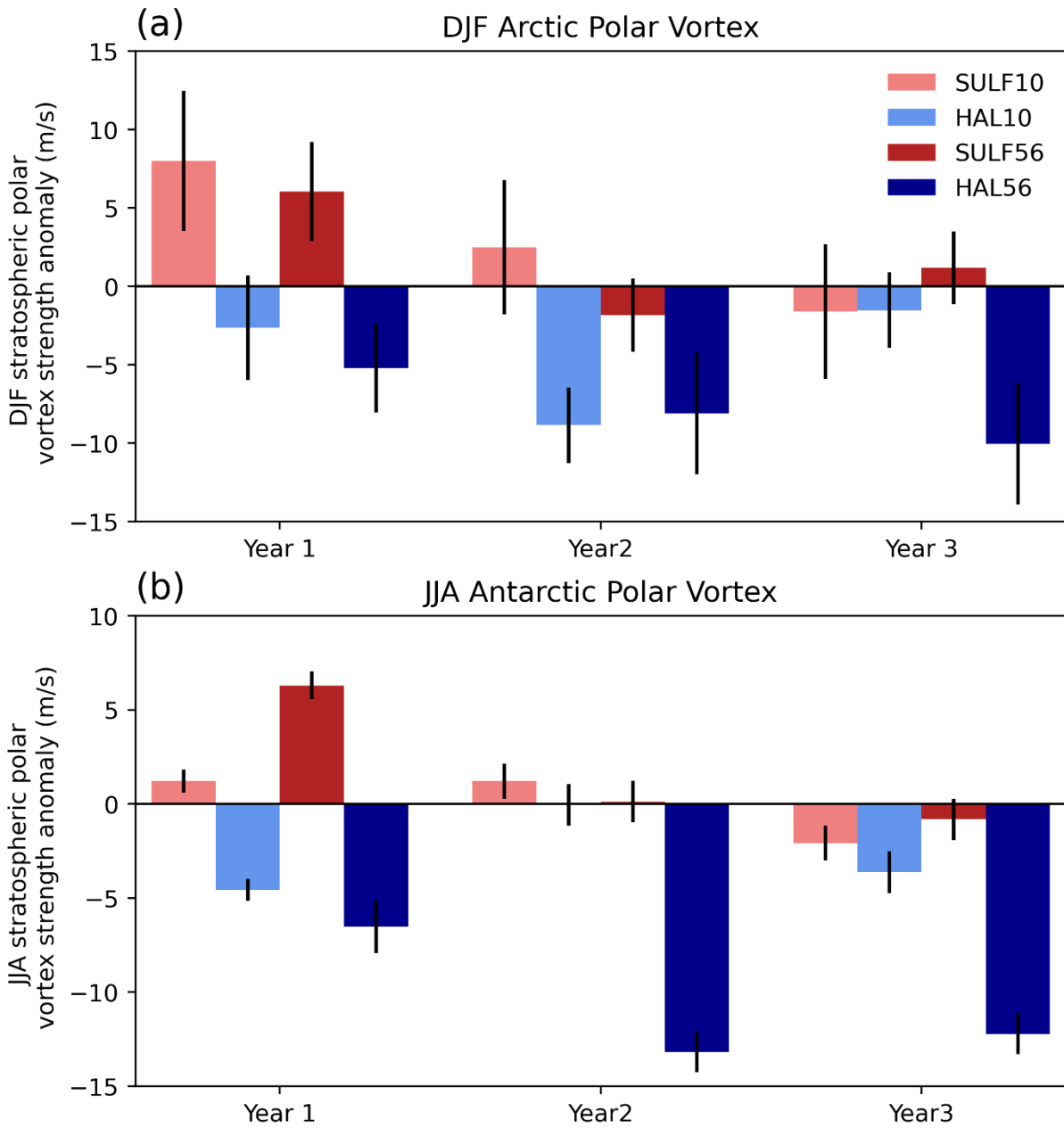
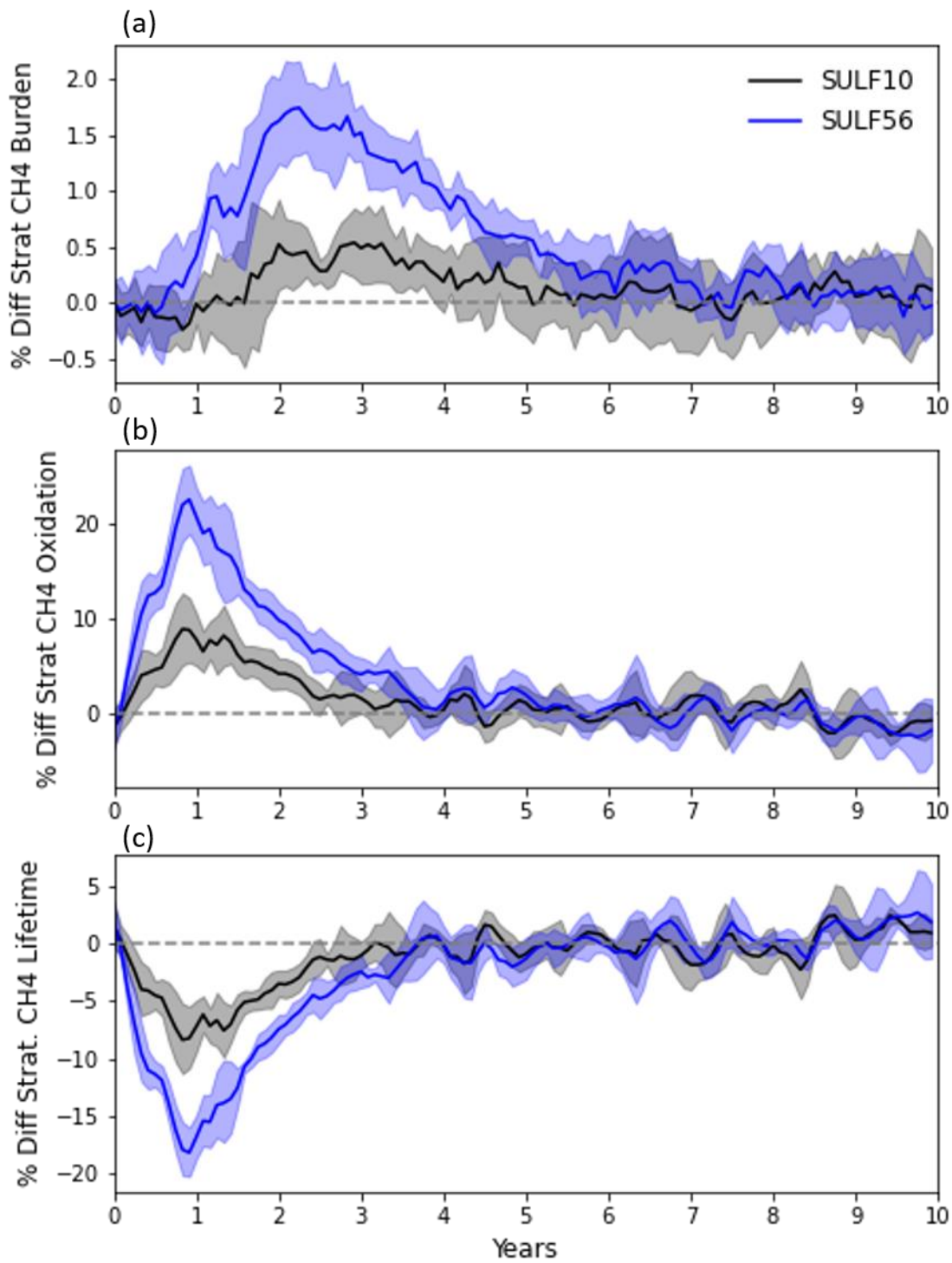


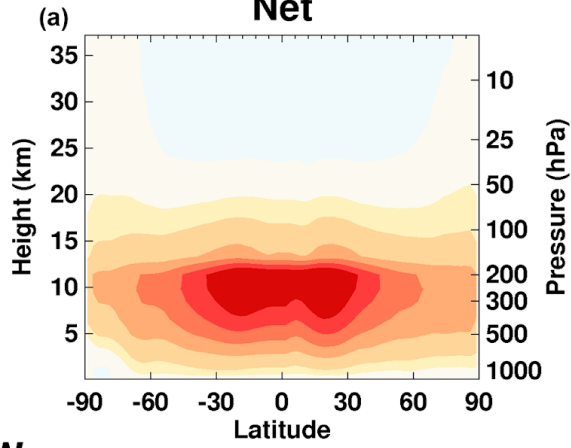
**Figure S7** Polar vortex strength in the northern hemisphere winter (DJF) (a) and southern hemisphere winter (JJA) (b) in the first 3 post eruption years. The polar vortex strength was defined as the zonal mean wind speed averaged over 55°-65° and 1-30hPa. Error bars show one standard deviation across the ensemble.



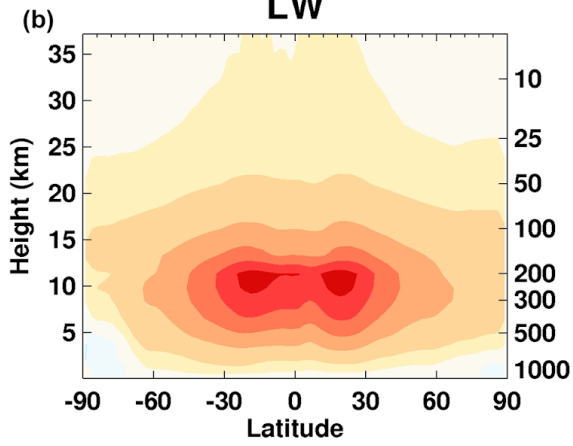
35 **Figure S8** Timeseries of percentage change in stratospheric methane burden (a), stratospheric methane oxidation flux (b) and stratospheric methane lifetime (c). Shading represents the ensemble range.

$O_3$  RK [ $mWm^{-2} / ppbv / 100 hPa$ ]

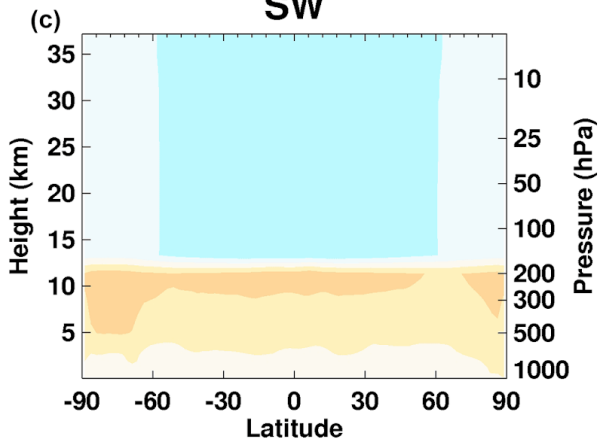
**Net**



**LW**



**SW**



40

**Figure S9** Annual zonal mean whole atmosphere ozone radiative kernel from (Rap et al., 2015) under all-sky conditions for (a) net (LW + SW), (b) LW, and (c) SW components. Figure taken from Iglesias-Suarez et al. (2018).

45

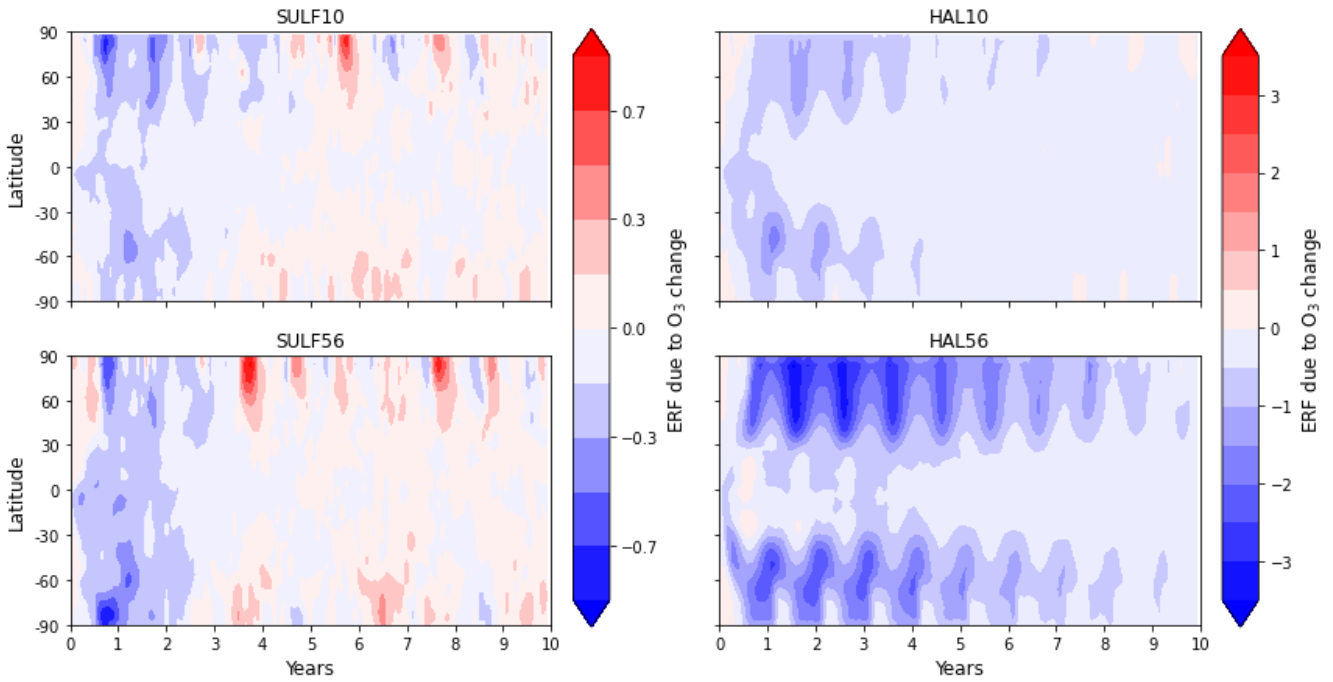


**Figure S10** Evolution of the TOA net flux anomalies due to stratospheric ozone change in SULF10, HAL10, SULF56 and HAL56 estimated from the ozone radiative kernel from Rap et al. (2015). Increases in TOA net forcing are shown in shades of red, and decreases in shades of blue.

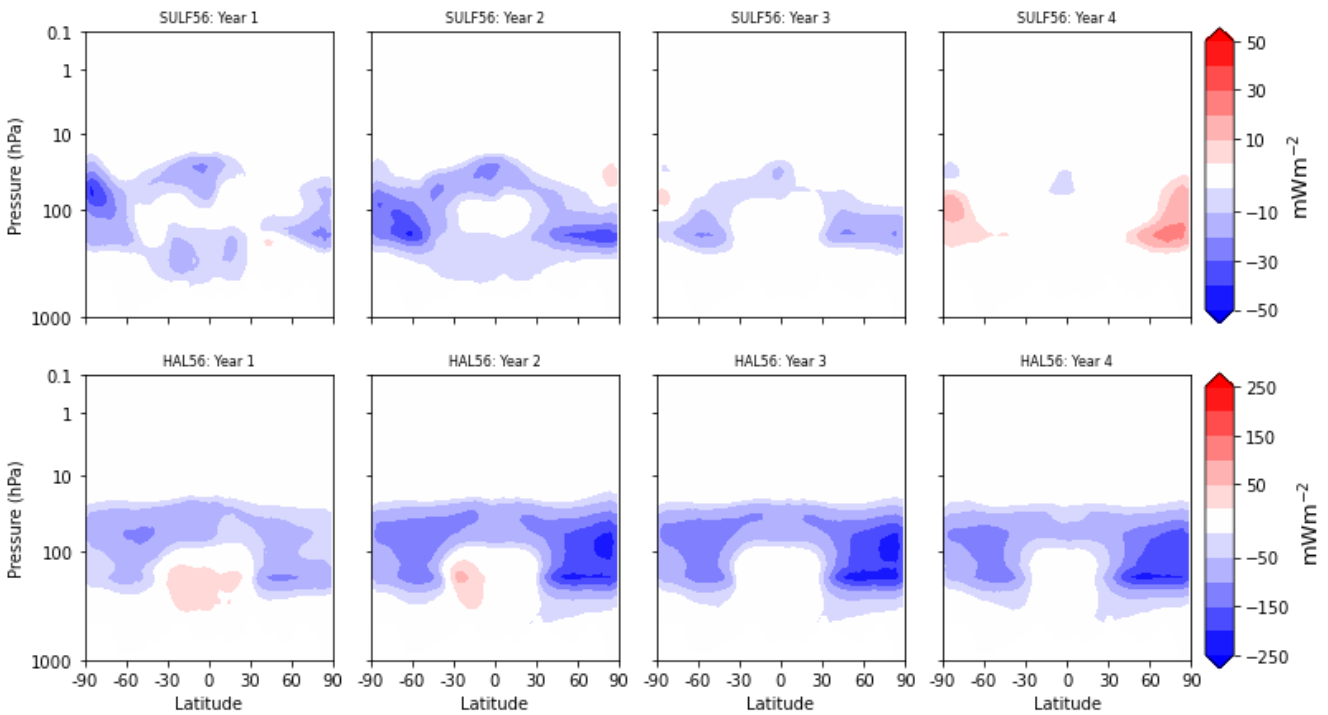


**Figure S11** Zonal mean difference in TOA net flux anomalies for the first four post eruption years due to stratospheric ozone change in SULF56 (top) and HAL56 (bottom) estimated from the ozone radiative kernel from Rap et al. (2015). Increases in net forcing are shown in shades of red, and decreases in shades of blue.

55

60

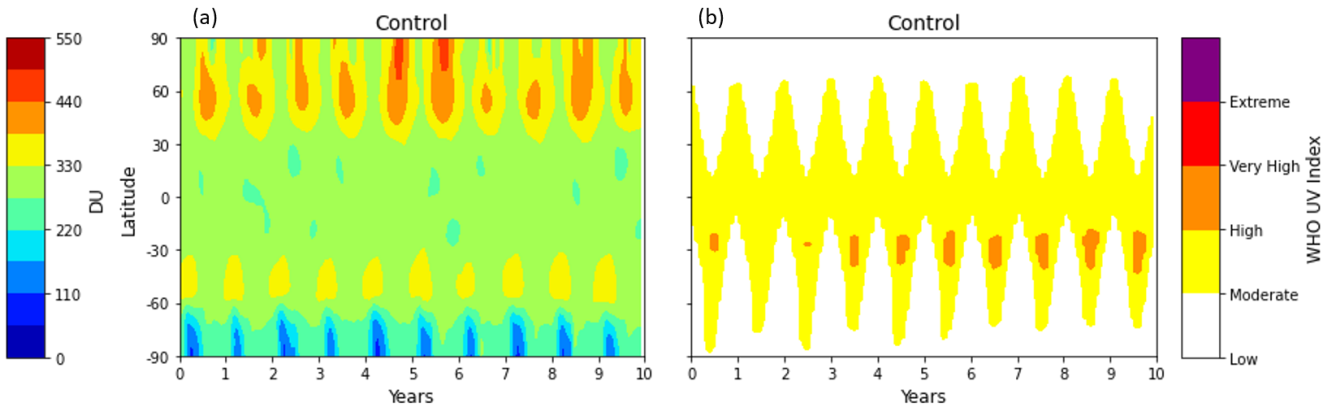


**Figure S12** Zonal mean column ozone (a) and zonal-mean daily average UV index (b) in the control simulation. Ozone hole conditions are simulated when the column ozone < 220 DU.

65

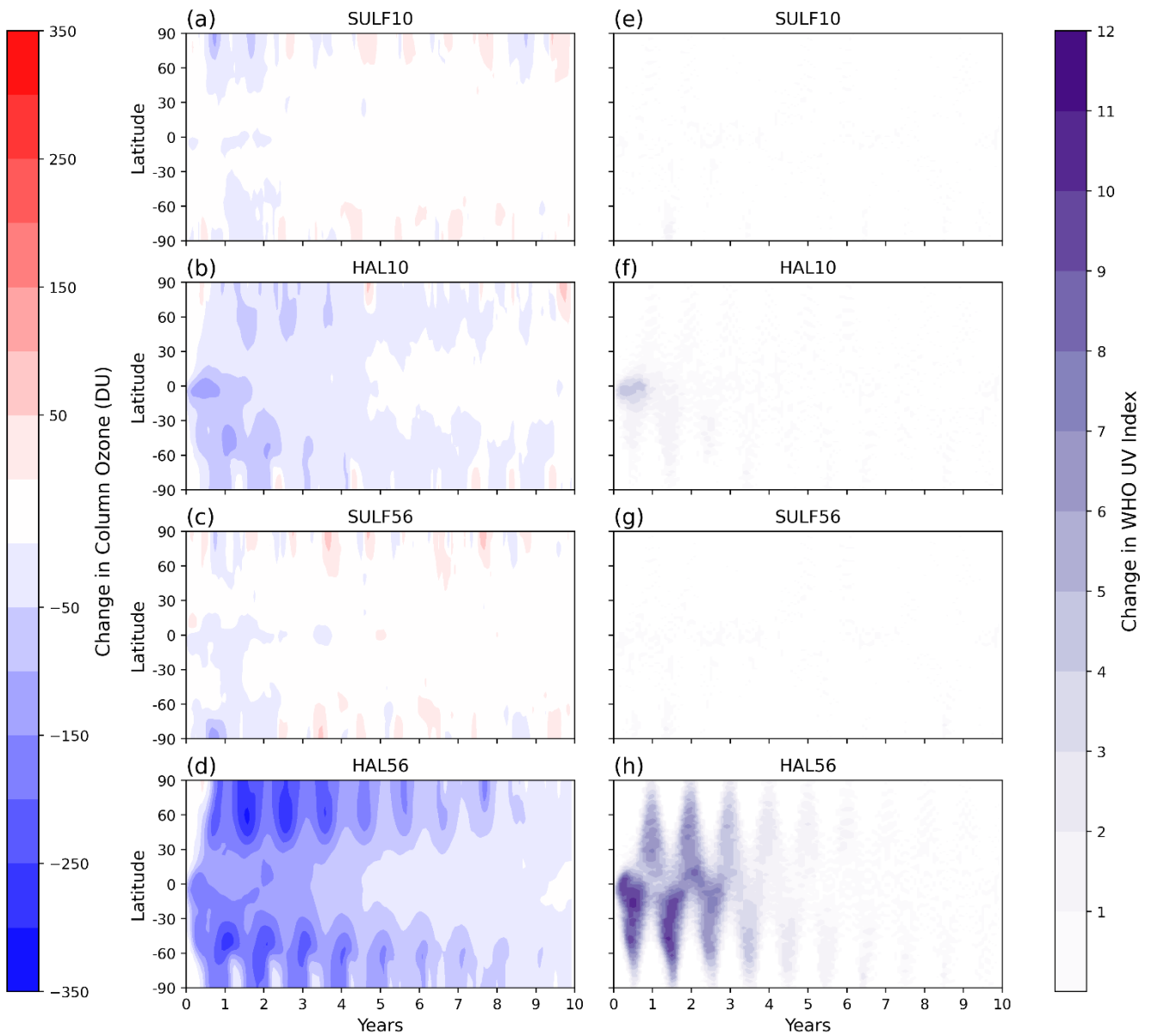


**Figure S13** Zonal mean change in column ozone (left) and Zonal mean change in the WHO UV index (right) in the control simulation.

